Electrical Properties of Silver-Silicone Rubber Nanocomposites for High-Voltage Outdoor Insulators

Lívia C. dos Passos Araújo, Maria E. Leyva, Estácio T. Wanderley Neto, and Alvaro A. A. de Queiroz

***Abstract*— Currently, the selection of high-temperature vulcanizing silicone rubber (HTVSiR) formulations resistant to the growth of microorganisms and which suitable electrical properties plays an important role in the manufacture of the polymeric high-voltage outdoor insulators (HVOIs) with high lifetime. In this work, silver-HTVSiR nanocomposites (AgHTVSiR) formulations are prepared and their electrical and antimicrobial properties are presented. Ag nanoparticles were electrochemically synthesized and characterized by scanning electron microscopy-energy dispersive spectrometry (SEM-EDS), UV-visible (UV-Vis), and X-ray (XRD) spectroscopies. Thermogravimetric (TG/DTG) analysis is undertaken with the purpose of determining the thermal behavior of AgHTVSiR. The complex impedance analyses were conducted to investigate the electrical conduction mechanism of the AgHTVSiR nanocomposites via electrochemical impedance spectroscopy (EIS) within a frequency range from 0.1 Hz to 0.1 MHz. XRD revealed Ag nanoparticles of 50 nm in diameter size. The images of SEM-EDS evinced the homogeneity of Ag nanoparticles dispersion into the HTVSiR matrix. The incorporation of silver nanoparticles does not change the thermal stability of the AgHTVSiR nanocomposite as compared to neat HTVSiR. The AgHTVSiR nanocomposites have maximal values for real part (Z') at low frequencies. Z' is found to decrease as the frequency of the applied alternating electric field increases. Furthermore, there is an improvement in the permittivity values for the AgHTVSiR nanocomposites with an increase in the concentration of 0.1 wt.%–0.3 wt.% of the Ag nanoparticles. Also, the AgHTVSiR shows excellent antimicrobial efficacy against *Trichoderma spp* fungus. The impedance characteristics of the AgHTVSiR nanocomposite along with its high dielectric permittivity and excellent antimicrobial property make it suitable for application in HVOI.**

***Index Terms*— Dielectric constant, electrochemical impedance spectroscopy (EIS), nanocomposites, rubber, silicon, silver.**

I. Introduction

HIGH-TEMPERATURE vulcanizing silicone rubber (HTVSiR) is acommercially available elastomer widely employed in the manufacture of high-voltage outdoor insulators (HVOIs) for use in power engineering due to its low surface energy, highly hydrophobic surface, and excellent resistance to the weather [1]. Nowadays, HVOI plays a vital role in the efficient and reliable transmission of electrical power around the world.

It is a well-known fact that when HVOI insulators based on HTVSiR are energized and exposed to polluted environments under different climatic conditions, microorganism biofilms are formed along their surface causing a considerable degradation in their insulating performance [2].

The fungal colonization and biofilm formation may result in a drastic reduction of the HTVSiR surface hydrophobicity increasing the electrical discharges and flash-over currents and reduces drastically the lifetime of the HVOI device [3], [4]. Fig. 1 shows a typical HTVSiR-based HVOI colonized by the *Trichoderma spp* fungal.

Various compounds have been used as antimicrobial agents in HTVSiR formulations, ranging from isothiazolone biocides to essential oils metal ions and nanoparticles [5], [6]. In recent years, there has been a great deal of interest in the development of more environmentally friendly and less toxic materials due to the risks of the traditional biocides to humans and the environment. Nowadays, metal-based nanoparticles, such as silver, zinc, and copper nanoparticle types, have shown demonstrated their potential as efficient antimicrobial agents in HTVSiR [7].

Silver nanoparticles (Ag) today are a promising antimicrobial to control biofilm formation as they offer prolonged antimicrobial activity with negligible toxicity, compared with the classic antimicrobial agents that display short-term activity and human or environmental toxicity [8].

Manuscript received 28 July 2023; revised 17 November 2023 and 13 December 2023; accepted 27 December 2023. Date of publication 2 January 2024; date of current version 31 May 2024. This work was supported in part by the National Council for Scientific and Technological Development (CNPq) and in part by the Coordination of Superior Level Staff Improvement (CAPES). The work of Alvaro A. A. de Queiroz was supported by CNPq under Grant 307609/2018-9. *(Lívia C. dos Passos Araújo, Maria E. Leyva, Estácio T. Wanderley Neto, and Alvaro A. A. de Queiroz contributed equally to this work.) (Corresponding author: Alvaro A. A. de Queiroz.)*

Lívia C. dos Passos Araújo and Maria E. Leyva are with the Physics and Chemistry Institute, Federal University of Itajubá (UNIFEI), Itajubá 37500-903, Brazil (e-mail: livia.cecilia@unifei.edu.br; mariae@unifei.edu.br).

Estácio T. Wanderley Neto is with the High Voltage Laboratory Prof. Manuel Luís Barreira Martinez (LAT-EFEI), Federal University of Itajubá (UNIFEI), Itajubá 37500-903, Brazil (e-mail: estacio@unifei.edu.br).

Alvaro A. A. de Queiroz is with the Nuclear and Energy Research Institute-IPEN, Cidade Universitária Armando de Salles Oliveira, Butantã, São Paulo 05508-000, Brazil (e-mail: alvaro.queiroz@ipen.br).

Color versions of one or more figures in this article are available at https://doi.org/10.1109/TDEI.2023.3349256.

Digital Object Identifier 10.1109/TDEI.2023.3349256

Fig. 1. Rod insulators based on SiR commonly applied to high-voltage (15 kV) power line to support conductor and insulate from ground (a) before use and (b) after nearly five years in operation at the altitude of 850 m, temperate climate with annual rainfall precipitation of 1375 mm, and average temperature of 21 °C in the region of Itajubá, Minas Gerais-Brazil. The arrows indicate some of the points of the insulator colonized by microorganism *Trichoderma spp.*

Numerous studies have shown the interest of using Ag fillers in the silicone rubber (SiR) with antimicrobial activity for medical device applications [8]. To the best of our knowledge, there have been no studies regarding the dielectric and electrical properties of Ag-filled HTVSiR for HVOI applications.

In the present scenario, HVOI with improved dielectric and antimicrobial properties is in great demand. In the present work, AgHTVSiR nanocomposites were produced and their dielectric behavior was explored at different Ag loadings. The idea is to obtain an AgHTVSiR nanocomposite with good electrical and antimicrobial performance but also with the minimum contribution of Ag needed to achieve this goal. The effect of Ag nanoparticles has been explored on the real (Z') and imaginary (Z'') parts of impedance and the Nyquist plot of the AgHTVSiR nanocomposite films. The morphology and antimicrobial properties of the AgHTVSiR were also studied as will be discussed in the following.

II. Experiment: Materials and Methods

A. Electrochemical Synthesis of Silver Nanoparticles

The synthesis of silver nanoparticles (Ag) was performed in a simple two-electrode cell by using an Autolab PGSTAT302N (Metrohm) potentiostat. The electrolytic cell consists of platinum electrodes of different dimensions, a plate ($2.0 \times 0.5 \times 0.1$ cm) as an anode, and a wire (5×0.1 cm) as a cathode. The electrolytic solutions consisted of SiO_2 (5.0 mM) dispersed in KNO_3 (0.1 M) and $AgNO_3$ (5.0 mM). The electrolytic cell was kept inside an ultrasonic bath and the electrolysis was carried out in galvanostatic mode at cathodic current density of 9.6 mA/cm^2 at room temperature (25 °C).

The synthesized Ag nanoparticles were centrifuged at 3000 r/min for 30 min, removing the supernatant, and the pellets were redispersed twice in distilled and deionized water and then centrifuged again at 3000 r/min for 30 min. The purified Ag pellets were lyophilized (Imautomatiche, Minifast 04) overnight for use. The Ag was characterized by UV-visible spectroscopy (UV-Vis, Cary 50, Varian) and X-ray diffractometry (XRD, Rigaku, Ultima IV, 40 kV, 50 mA, CuKα line at 1.54056 Å) techniques.

B. Preparation and Characterization of the AgHTVSiR

The Ag@SiO_2 filled HTVSiR compound was prepared by a two-step mixing method. First, the HTVSiR (1.0 g) and the Ag@SiO_2 (0.1 wt.%–0.3 wt.%) were manually mixed together for 30 min at room temperature (25 °C). Finally, the AgHTVSiR nanocomposite was transferred into a mold of 0.6 cm in diameter and 0.1 cm thickness and then was cured at 180 °C for 24 h under a pressure of 2.2 MPa, as HTVSiR manufacturer's recommended. The cured AgHTVSiR nanocomposite was taken out from the mold and measured for its homogeneity in nanoparticle distribution, hydrophobicity, thermal stability, and electrical properties.

The physical chemistry characterization using attenuated total reflection Fourier transform infrared (ATR-FTIR) spectroscopy allows analyzes the chemical groups on polymeric surface of the sample's studies. The calculated penetration depth of ATR is around 0.664 μm. Therefore, we correlated the intensity of transmittance peaks in the ATR-FTIR spectrum with the concentration of chemical groups on polymer surface, using a peak as internal reference. ATR-FTIR spectroscopy was realized through FTIR Shimadzu IRTracer 100 spectrometer provided by an ATR diamond accessory. The spectrum was obtained on transmittance mode and was scanned registering the spectrum with 30 scans at a resolution of 4 cm^{-1}, from 4000 to 650 cm^{-1}.

The distribution of the Ag@SiO_2 in the HTVSiR matrix was evaluated by scanning electron microscopy (SEM, Zeiss Evo MA15) equipped with an energy-dispersive spectrometer (SEM-EDS). Surface hydrophobicity of the AgHTVSiR nanocomposite was examined by water contact angle measurements (WCA) using a contact angle goniometer (DSA20E, KRUSS) and water as probe liquid.

The thermal stability of the AgHTVSiR nanocomposite was studied by thermogravimetric analysis (TGA, Shimadzu TGA-50) at a heating rate of 10 °C·min^{-1} from 25 °C to 900 °C under nitrogen gas (flow rate: 20 mL·min^{-1}). The effect of the Ag@SiO_2 on thermal transitions of cured HTVSiR was studied by differential scanning calorimetry (DSC) (Shimadzu Calorimeter, DSC model 60 Plus). The experimental procedure was realized cooling the calorimeter from 25 °C to −120 °C and then heated from −120 °C to 25 °C at a rate of 10 °C/min. All scans were carried out under a nitrogen atmosphere at a rate of 50 mL/min.

The electrical properties of the AgHTVSiR nanocomposite were evaluated by electrochemical impedance spectroscopy (EIS) measurements. The EIS measurements were performed using an Autolab PGSTAT302N (Metrohm) in a frequency range from 0.1 Hz to 0.1 MHz. The AgHTVSiR samples were held in the dielectric cell between two parallel gold-plated electrodes. The amplitude of the alternating electric current signal applied to the samples was 1 V. The electrical resistivity was determined using two-probe measurements. The

current–voltage (I–V) characteristics at room temperature (25 °C), within a voltage sweep of 0–0.02 V, were obtained using a Keithley 2636A dual channel source. To study I–V characteristics, Ag ink was used in the two faces of the cylindrical samples, with a cross-sectional area of 0.283 cm^2 and thickness of 0.1 cm.

C. Microbiological Assay of AgHTVSiR

The unmodified HTVSiR served as control. Disk-shaped specimens for the microbial tests were obtained by punching the foils with a 12-mm steel punch. Ring-shaped specimens with an outer diameter of 58 mm and an inner diameter of 50 mm were produced with a precision steel punch to investigate the antifungical properties of the AgHTVSiR nanocomposite.

The isolates of the fungus *Trichoderma spp.* were obtained from the commercial HVOI of company Energisa, which has been in operation in the region of Itajubá-MG- Brazil, for five years. A spore suspension was prepared by growing the *Trichoderma spp* for 14 days on a potato-dextrose-agar (PDA) culture medium. The plates were kept in a biochemical oxygen demand growth chamber (BOD, SPLabor) at a temperature of 25 °C ± 2 °C. The spores were transferred to a sterile bottle. The spore concentration was determined and a mixed suspension was prepared, so that in the mixture, the concentration of 10^6 conidia·mL^{-1} was reached. The materials were inoculated by spraying 0.3-mL suspension onto the samples, giving around 10^4 conidia·cm^{-2} surface of the samples. The inoculated test specimens and controls were covered and incubated at 28 °C and 85% relative humidity for 28 days. Fungal growth on the materials was examined visually each week during the experiment following the guidelines given in ASTM G21-13 [9]. Data were expressed as growth inhibitory zone diameter (cm) for three replicates.

III. Results and Discussion

A. Physicochemical Characterization of the AgHTVSiR

ATR-FTIR spectroscopy was carried out on the surface of the SiO_2, Ag@SiO_2, HTVSiR, and AgHTVSiR to identify the chemical functional groups at the surface of each material. Fig. 2(a) shows the FTIR spectrum of HTVSiR. The absorption peaks between 3000 and 3550 cm^{-1} are assigned to stretch bands of the O–H bond. The band at 2966 and 1251 cm^{-1} revealed the presence of methyl groups (-CH_3). The vibrational bands at 1090, 1009, and 786 cm^{-1} are assigned to O–Si–O bond of silicone matrix. Fig. 2(b) shows the FTIR spectrum of SiO_2 and Ag@SiO_2. Both spectra show the vibrational bands next to 1061 and 786 cm^{-1} typical of O–Si–O asymmetrical and symmetrical stretching bond, respectively. Fig. 2(c) shows the FTIR spectrum of AgHTVSiR. The absorption peaks of AgHTVSiR are the same to HTVSir sample.

The ratio between the intensity of -CH_3 absorption bands (2966 and 1251 cm^{-1}) of the side-chain group and absorption band of O–Si–O (1009 cm^{-1}) of the principal-chain group of the SiR was determined. The results (Fig. 2) suggest a higher concentration of methyl groups on the surfaces of AgHTVSiR samples compared to HTVSiR. This implies that the addition of Ag@SiO_2 provides the AgHTVSiR more hydrophobic due to the freely rotating of the methyl group into the bulk of the HTVSiR to the surface of the composite.

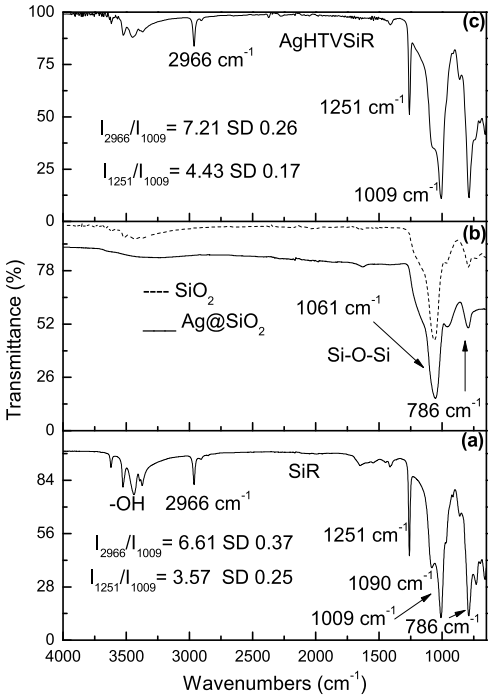

Fig. 2. (a) ATR-FTIR spectrum of SiR, (b) SiO_2 and Ag@SiO_2, and (c) AgHTVSiR. SD refers to the standard deviation error limit from three replicate measurements.

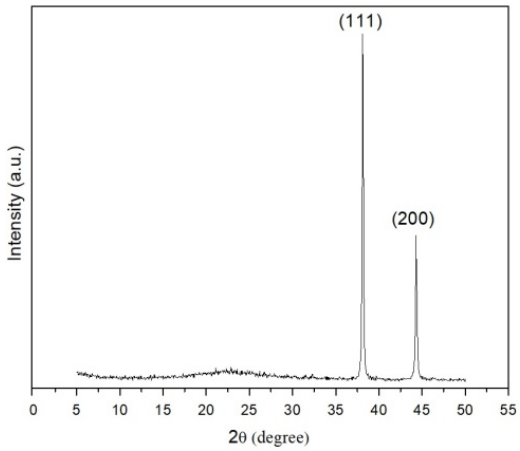

Fig. 3. XRD patterns of electrochemically synthesized silver nanoparticles.

The analysis of structure and crystalline size of the synthesized Ag was carried out by XRD (Fig. 3). The XRD analysis of synthesized Ag showed diffraction peaks at 38.1° and 44.3°, confirming the crystalline nature of the synthesized nanoparticles. The XRD peaks can be assigned to the planes (111) and (200) facet of silver crystal, respectively, and are in good agreement with JCPDS card number 04–0783. The full-width at half-maximum (FWHM) values was used to calculate the size of the Ag [10]. The average size of Ag was found to be around 43.8 nm.

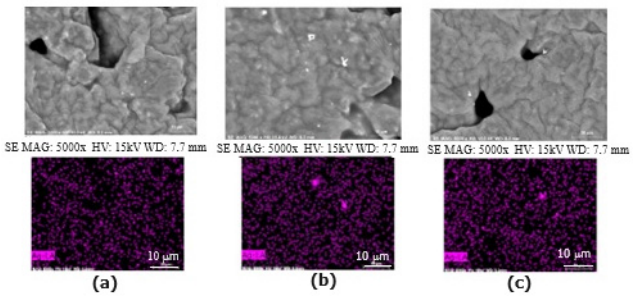

Fig. 4. Analysis of the Ag@SiO_2 distribution in the HTVSIR matrix at nanoparticles composition (wt.%) (a) 0.1%, (b) 0.2%, and (c) 0.3%.

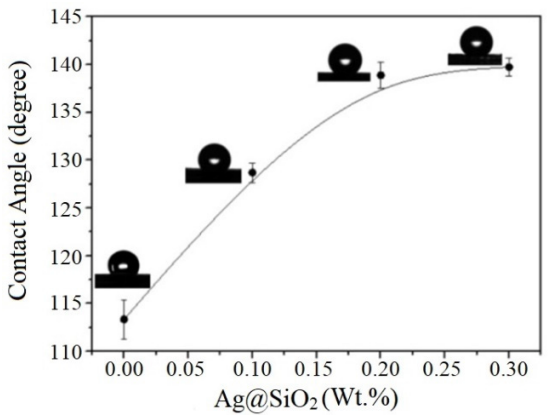

Fig. 5. Contact angles of the AgHTVSiR nanocomposite measured at room temperature (25 °C).

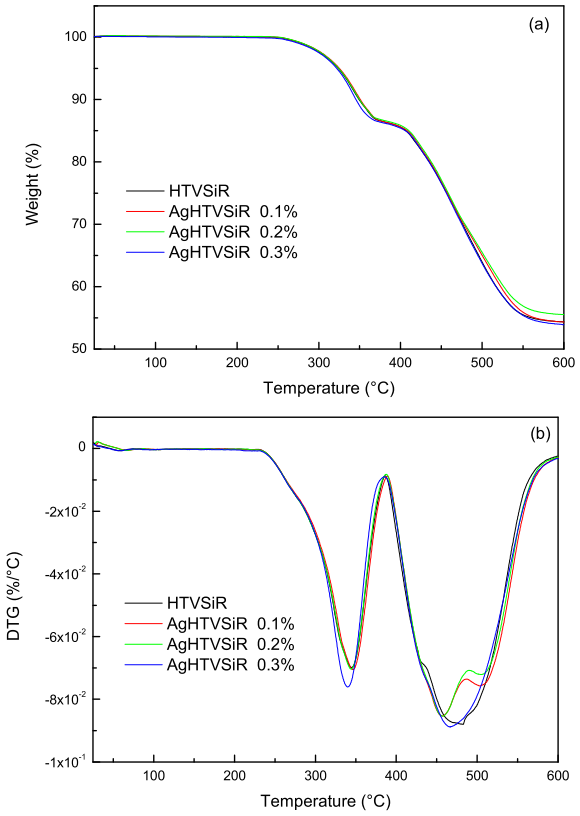

Fig. 6. Thermogravimetric analysis of AgHTVSiR nanocomposites (a) TG and (b) DTG.

The SEM-EDS analysis of the manufactured AgHTVSiR nanocomposites manifested a good dispersion and homogeneous distribution of Ag nanoparticles into a polymer matrix (Fig. 4). This is due to the mechanical technique, which in turn improves the dispersion of Ag@SiO_2 into HTVSiR, and the main factor increases the interaction between the nanoparticles and polymer matrix due to their size and high surface area.

The incorporation of Ag@SiO_2 into HTVSiR matrix is recommended due to their reported antifungal properties. However, this incorporation can affect the wettability of HVTSiR. The results of contact angle measurements of AgHTVSiR nanocomposites with water are presented in Fig. 4. The contact angle of the HTVSiR was significantly lower than that of the AgHTVSiR nanocomposites at all Ag@SiO_2 concentrations (Fig. 5), suggesting an increase in hydrophobicity of the HTVSiR matrix.

The increase in hydrophobicity of the HTVSiR with the addition of the Ag@SiO_2 (Fig. 5) can be explained by the increase of hydrophobic methyl groups on the surface of SiR matrix as was observed in the FTIR spectrum (Fig. 2) [11]. This fact could be responsible for the decrease in the surface energy of HTVSiR and therefore results in an increase in hydrophobicity of the AgHTVSiR nanocomposites and contact angle relatively to the HTVSiR matrix. Taking into account the applicability of the AgHTVSiR composition as insulating materials for HVOI, this increase of hydrophobicity becomes a positive point since the decrease of this property can lead to the increase of leakage current, being able to lead to the deterioration of the insulator [12].

Thermal stability is a very important property for HVTSiR used in the manufacture of HVOI, and therefore, the thermal stability of the AgHTVSiR nanocomposite was studied. The thermal stability of the pure HTVSiR and AgHTVSiR nanocomposites was investigated using TG/DTG, and the results are presented in Fig. 6. It is clear that the HTVSiR and AgHTVSiR nanocomposites at different Ag@SiO_2 compositions showed no significant difference in the value of thermal stability from each other.

The TG/DTG indicated two prominent phases in the thermal degradation behavior of the HTVSiR and AgHTVSiR nanocomposites (Fig. 6). The first phase starts at 230 °C and ends at 386 °C with around 15% weight loss, suggesting the evaporation of the crystal water molecules in alumina trihydrate (ATH) [13]. ATH has been commonly used as a fire retardant in commercial HTVSiR formulations [14]. The second phase of TGA analysis (Fig. 6) starts at 386 °C and ends at 574 °C with around 40% weight loss indicating the second stage of crystalline water molecules liberation of ATH and depolymerization of HTVSiR matrix [15]. The aluminum oxide (Al_2O_3) formed combined with the products of HTVSiR depolymerization appears to be responsible for the 55% residual mass observed in TGA analysis at 600 °C (Fig. 6) [16].

The DSC curve (Fig. 7) shows that melt temperature (T_m) and fusion enthalpy (endothermic process) (ΔH) values for different AgHVTSiR compositions are close to HVTSiR.

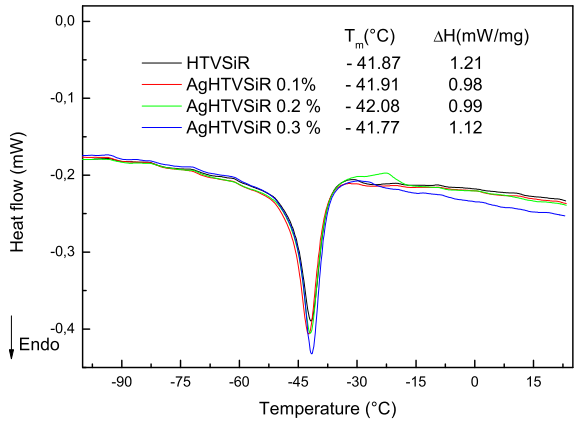

Fig. 7. DSC analysis of AgHTVSiR nanocomposites.

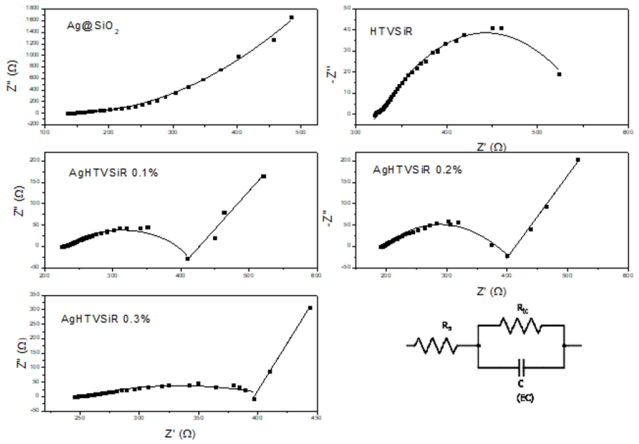

Fig. 8. Nyquist plot of AgHTVSiR nanocomposites as a function of $Ag@SiO_2$ loading at room temperature (25 °C) and their respective EC model.

The width of fusion peak is close for all samples. The DSC results obtained suggest that $Ag@SiO_2$ is not influence the fusion of polydimethylsiloxane (PDMS) segments in HVTSiR. Therefore, confirms that there is a homogeneous distribution of the $Ag@SiO_2$ in HVTSiR matrix, as observed in the SEM micrograph (Fig. 4).

B. Impedance Analysis

EIS was used to understand the conduction and relaxation mechanism of the AgHTVSiR nanocomposites in the range of 0.1 Hz–0.1 MHz. Fig. 8 represents the Nyquist plots of HTVSiR and AgHTVSiR nanocomposites. All systems studied through the Nyquist diagrams were fitted to the equivalent circuit (EC) shown in Fig. 8. The Nyquist plot of the AgHTVSiR nanocomposites (Fig. 8) shows the tendency of the system to form low-amplitude asymmetric semicircular arcs at high frequencies regions followed by a linear behavior in the low-frequency region. The amplitude of the semicircular arcs decreases with the increase in the Ag weight fraction (wt.%) and is indicative of the capacitive behavior of the system. The observed asymmetry of the semicircular arcs is indicative of non-Debye type of relaxation with different times, probably due to the nanosized gaps between the conductive

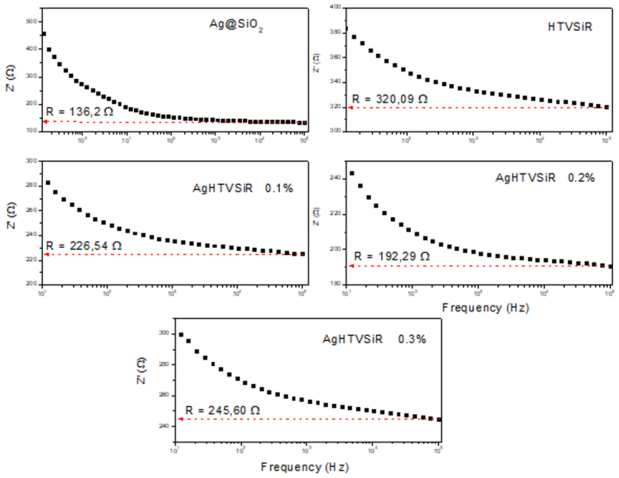

Fig. 9. Variation of imaginary part of impedance with frequency for AgHTVSiR nanocomposites and HTVSiR at room temperature (25 °C).

channels that are responsible for the nonohmic conduction of electrons [17].

The linear region observed in EIS of AgHTVSiR nanocomposites (Fig. 9) suggests an electrolyte resistance (R_s) associated with the charge transfer due to the diffusion of the electrolytic medium [18]. For HTVSiR (Fig. 9), R_s was not observed, and the arc impedance semicircle of greater diameter suggests a system with high resistance R_{tc}. The impedance semicircle arc was not formed in the $Ag@SiO_2$ (Fig. 8), suggesting the strong influence of the diffusional component correspondent to the lower resistance value R_{tc}.

The variation of real part of the impedance with the frequency of the AgHTVSiR is shown in Fig. 9. For all $Ag@SiO_2$ compositions, the (Z') values are found to decrease with increasing frequency. The maximum values of Z' of all AgHTVSiR compounds have been recorded at low-frequency range, which may indicate an accumulation of a space charge polarization. The decrease in impedance at higher frequencies (Fig. 9) may be attributed to the hopping of electrons between localized ions.

The resistance value between the circuit contacts, i.e., the series resistance [$R_{s(ac)}$], of the HTVSiR and AgHTVSiR nanocomposites to the alternating current (ac) was calculated by extrapolating the saturated region of the impedance to the Z'-axis (Fig. 7). Considering $R_{s(ac)}$, the corrected capacitance (C_{corr}) can be expressed in terms of Z' and Z'' as follows [18]:

$$C_{\text{corr}} = -\frac{1}{\omega}\left[\frac{Z''}{\left(Z' - R_{s(ac)}\right)^2 + (Z'')^2}\right] \quad (1)$$

where ω is the angular frequency ($\omega = 2\pi f$) and $R_{s(ac)}$ is the value of the series resistance (Fig. 9).

The capacitance (C_{corr}) for the AgHTVSiR nanocomposites is shown in Fig. 10. It may be noted that the capacitance of the Ag@ is more affected by the frequency than AgHTVSiR, suggesting a greater number of interfaces in the nanocomposites and therefore more regions that can store and polarize load conveyors. Moreover, $Ag@SiO_2$ exhibits higher capacitance relatively to the AgHTVSiR nanocomposites (Fig. 10).

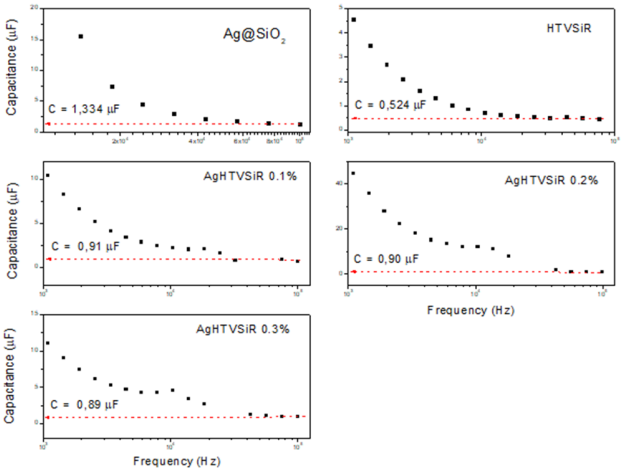

Fig. 10. Influence of the Ag nanoparticles (wt.%) on capacitance of the AgHTVSiR nanocomposites at room temperature (25 °C).

TABLE I
CAPACITANCE AND PERMITTIVITY VALUES AT 0.1 MHz FOR AgHTVSiR AS A FUNCTION OF $Ag@SiO_2$ COMPOSITION

$Ag@SiO_2$ (wt.%)	Capacitance (µF)	Dielectric constant (ε)
100	1.334	7.92
HTVSiR	0.524	3.11
0.1	0.91	5.40
0.2	0.90	5.34
0.3	0.89	5.28

The loads stored at the interfaces of the AgHTVSiR nanocomposites cannot be polarized in the ac electric field and the values of C_{corr} do not appear to contribute to the capacitance of the system.

Changing the polarization, the saturation value of capacitance at high frequencies remains constant regardless of the applied voltage (AV) and the value of the corrected capacitance (C_{corr}) at high frequencies can be considered similar to the geometric capacitance (C_g) of the AgHTVSiR analyzed in the measurement cell.

The geometric capacitance (C_g) can be obtained from the extrapolation in the saturation region of the capacitance and the dielectric constant of the AgHTVSiR nanocomposites can be calculated in according to the following equation:

$$\varepsilon = \frac{C_g d}{\varepsilon_0 A} \tag{2}$$

where ε_0 is the vacuum permittivity (8.85. 10^{-14} F/cm), d is the thickness of the double layer (distance of the electrode/sample interface, 1.03 × 10^{-7} cm), and A is the area of the electrode (0.196 cm^2).

The values of the capacitance (C) and permittivity (ε) for $Ag@SiO_2$, HTVSiR, and AgHTVSiR nanocomposites at room temperature (25 °C) are shown in Table I. The HTVSiR exhibits low ε, and this could be due to its crosslinked network nature. As the structure of HTVSiR becomes more oriented due to the crosslinking reactions, the less electrical polarization will occur decreasing the permittivity of the polymer matrix [19].

TABLE II
ELECTRICAL RESISTIVITY FROM I–V CURVE FOR AgHTVSiR AS A FUNCTION OF $Ag@SiO_2$ COMPOSITION

Samples	HTVSiR	AgHTVSiR		
		0.1%	0.2%	0.3%
$\rho*10^{11}$ (Ω.m)	1.64	1.23	1.03	1.30
$\sigma*10^{-12}$ ($S.m^{-1}$)	6.10	8.13	9.71	7.69

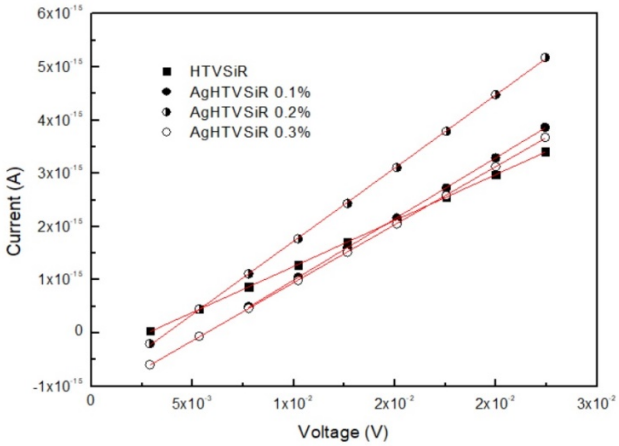

Fig. 11. Representative current–voltage curves for the AgHTVSiR nanocomposites with 0.1 wt.%, 0.2 wt.%, and 0.3 wt.% $Ag@SiO_2$ content. Measurements were made at room temperature (25 °C).

It is clearly seen (Table II) that the addition of $Ag@SiO_2$ increased ε of the HTVSiR, which originates from the remarkable interface polarization between the HTVSiR matrix and $Ag@SiO_2$ phases [20]. This change trends well matches with the variation of capacitance values (Table II). This result suggests that $Ag@SiO_2$ at lower concentration can be filled into the gaps between HTVSiR chains [21]. In this case, more $Ag@SiO_2$ per volume unit can result in a greater dipole moment, which will improve the dielectric permittivity of the HTVSiR matrix [22]. Since the individual permittivity of $Ag@SiO_2$ is higher than that of HTVSiR matrix, they will influence the values of the resultant permittivity of the AgHTVSiR, enhancing the homogeneity and distribution of the electric field on the surface and contributing to a decrease in the leakage current of the nanocomposites. Table I shows that the effect of $Ag@SiO_2$ concentration in the HTVSiR matrix is dispersible, in the range studied.

The electrical I–V measurements for the different AgHTVSiR nanocomposite samples are shown in Fig. 11. The electrical resistivity (ρ) was calculated from I–V curves using Ohm's law. The resistivity (ρ) and conductivity (σ) values were calculated in according to the following equation:

$$\rho = \frac{1}{\sigma} = \frac{R.A}{L} \tag{3}$$

where $A(m^2)$ is the cross-sectional cylindric area and L(m) is the thickness of AgHTVSiR samples.

Based on Fig. 11, the resistance values are derived from current and voltage readings across AgHTVSiR samples.

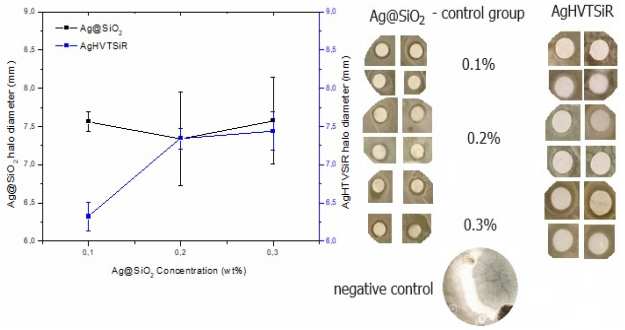

Fig. 12. Results of the disk diffusion test for *Trichoderma spp* after 28 days of incubation. Ag@SiO_2 as a control group and AgHTVSiR, both with 0.1%, 0.2%, and 0.3% concentration of Ag@SiO_2. The upper image illustrates the inhibition halos observed.

The electrical conductivity of pure HTVSiR and AgHTVSiR nanocomposites (wt % 0.10, 0.20, 0.30) is found to be $6.10.10^{-12}$, $8.1.10^{-12}$, $9.7.10^{-12}$, and $7.7.10^{-12}$ $S{\cdot}m^{-1}$ (Table II), respectively. It is evident that the weight % of Ag@SiO_2 does not exert a significant influence on the conductivity of HTVSiR since its value remains in the same order of magnitude (10^{-12} $S{\cdot}m^{-1}$). On the other hand, the AgHTVSiR nanocomposite exhibits resistivity (ρ) values as high as $1.23.10^{11}$, $1.03.10^{11}$, and $1.30.10^{11}$ $\Omega{\cdot}m$ (Table II) in the range of 0.1 wt.%–0.3 wt.% and can be classified as insulating materials.

C. Antimicrobial Activities

Antimicrobial activity of the AgHTVSiR disk diffusion tests was performed to investigate the antimicrobial efficacy of Ag nanoparticles at different concentrations, and the results are presented in Fig. 12. It is demonstrated that the Ag@SiO_2 concentrations between 0.1 wt.% and 0.3 wt.% could effectively inhibit the growth of *Trichoderma spp* (Fig. 10), and a large zone of inhibition of the microorganism was still present after 28 days of incubation.

IV. Conclusion

In this study, HTVSiR nanocomposites with different concentrations of silver nanoparticles were prepared. Electrochemical synthesis method was used to synthesize the silver nanoparticles with an average size of 43.8 nm. SEM-EDS analysis confirmed that Ag nanoparticles were homogeneously dispersed at HTVSiR matrix. The introduction of Ag nanoparticles increases the permittivity of the HTVSiR nanocomposite mainly due to the influence of Ag nanoparticles permittivity. Through the static water contact angle analysis, it was observed that with the increase Ag nanoparticles composition in the polymer matrix, there is an increase in the degree of hydrophobicity of the HTVSiR formulations. It was noted that the thermal stability of HTVSiR was not significantly altered from the compositions ranging from 0.1 wt.% to 0.3 wt.%, confirming the positive effect of the Ag nanoparticles on the thermal stability of the AgHTVSiR. The AgHTVSiR shows relatively higher dielectric permittivity than the HTVSiR matrix, which satisfies the applications of the nanocomposite in the field of power engineering. The antimicrobial tests showed good effect of AgHTVSiR nanocomposites against the fungus *Trichoderma spp*.

References

[1] F. Z. Kamand et al., "Self-healing silicones for outdoor high voltage insulation: Mechanism, applications and measurements," *Energies*, vol. 15, no. 5, p. 1677, Feb. 2022.

[2] Q. He et al., "Research progress of self-cleaning, anti-icing, and aging test technology of composite insulations," *Coatings*, vol. 12, pp. 1–33, Aug. 2022.

[3] L. Maraaba, K. Al-Soufi, T. Ssennoga, A. Memon, M. Worku, and L. Alhems, "Contamination level monitoring techniques for high-voltage insulators: A review," *Energies*, vol. 15, no. 20, p. 7656, Oct. 2022.

[4] J. Wang, S. M. Gubanski, J. Blennow, S. Atarijabarzadeh, E. Stromberg, and S. Karlsson, "Influence of biofilm contamination on electrical performance of silicone rubber based composite materials," *IEEE Trans. Dielectr. Electr. Insul.*, vol. 19, no. 5, pp. 1690–1699, Oct. 2012.

[5] S. Atarijabarzadeh, C. S. Lacamprett, S. Karlsson, and E. Strömberg, "Use of essential oils for the prevention of biofilm formation on silicone rubber high voltage insulators," *Polym. From Renew. Resour.*, vol. 6, no. 4, pp. 119–135, Nov. 2015.

[6] S. Atarijabarzadeh, E. Strömberg, and S. Karlsson, "Inhibition of biofilm formation on silicone rubber samples using various antimicrobial agents," *Int. Biodeterioration Biodegradation*, vol. 65, no. 8, pp. 1111–1118, Dec. 2011.

[7] T. Fischer, S. Suttor, S. Mansi, L. Osthues, and P. Mela, "Antimicrobial silicone rubbers based on photocatalytically active additives," *J. Appl. Polym. Sci.*, vol. 138, no. 46, pp. 1–11, Dec. 2021.

[8] C. M. Crisan, T. Mocan, M. Manolea, L. I. Lasca, F.-A. Tăbăran, and L. Mocan, "Review on silver nanoparticles as a novel class of antibacterial solutions," *Appl. Sci.*, vol. 11, no. 3, p. 1120, Jan. 2021.

[9] M. F. Aizamddin et al., "Synthesis, characterization and antibacterial properties of silicone-silver thin film for the potential of medical device applications," *Polymers*, vol. 13, pp. 1–16, Nov. 2021.

[10] *Standard Practice for Determining Resistance of Synthetic Polymeric Materials to Fungi*, ASTM Int., West Conshohocken, PA, USA, 2021.

[11] F. T. L. Muniz et al., "The Scherrer equation and the dynamical theory of X-ray diffraction," *Acta Crystallogr. A, Found. Adv.*, vol. A72, pp. 385–390, May 2016.

[12] M. Amin, M. Akbar, and S. Amin, "Hydrophobicity of silicone rubber used for outdoor insulation (an overview)," *Rev. Adv. Mater. Sci.*, vol. 16, pp. 10–26, 2007.

[13] F. Zheng et al., "The surface structure of UV exposed polydimethylsiloxane (PDMS) insulator studied by slow positron beam," *Appl. Surf. Sci.*, vol. 283, pp. 327–331, Oct. 2013.

[14] S. Strekopytov and C. Exley, "Thermal analyses of aluminium hydroxide and hydroxyaluminosilicates," *Polyhedron*, vol. 25, no. 8, pp. 1707–1713, May 2006.

[15] R. Han, Y. Li, Q. Zhu, and K. Niu, "Research on the preparation and thermal stability of silicone rubber composites: A review," *Compos. C, Open Access*, vol. 8, Jul. 2022, Art. no. 100249.

[16] C. Chen, Z. Jia, W. Ye, Z. Guan, and Y. Li, "Thermo-oxidative aging analysis of HTV silicone rubber used for outdoor insulation," *IEEE Trans. Dielectr. Electr. Insul.*, vol. 24, no. 3, pp. 1761–1772, Jun. 2017.

[17] W. Xue et al., "Detection and characterization of thermal degradation of HTV silicone rubber used in high voltage composite insulator taking into account abnormal temperature heating," in *Proc. IEEE Int. Conf. High Voltage Eng. Appl. (ICHVE)*, Beijing, China, Sep. 2020, pp. 1–4.

[18] V. Raja, A. K. Sharma, and V. V. R. Narasimha Rao, "Impedance spectroscopic and dielectric analysis of PMMA-CO-P4VPNO polymer films," *Mater. Lett.*, vol. 58, no. 26, pp. 3242–3247, Oct. 2004.

[19] V. V. Brus, A. K. K. Kyaw, P. D. Maryanchuk, and J. Zhang, "Quantifying interface states and bulk defects in high-efficiency solution-processed small-molecule solar cells by impedance and capacitance characteristics," *Prog. Photovoltaics, Res. Appl.*, vol. 23, no. 11, pp. 1526–1535, Jan. 2015.

[20] E. Cho et al., "Characterization of mechanical and dielectric properties of silicone rubber," *Polymers*, vol. 13, no. 11, p. 1831, Jun. 2021.

[21] Z.-M. Dang, J.-K. Yuan, J.-W. Zha, T. Zhou, S.-T. Li, and G.-H. Hu, "Fundamentals, processes and applications of high-permittivity polymer–matrix composites," *Prog. Mater. Sci.*, vol. 57, no. 4, pp. 660–723, May 2012.

[22] F. Faiza et al., "Multi-stressed nano and micro-silica/silicone rubber composites with improved dielectric and high-voltage insulation properties," *Polymers*, vol. 13, no. 9, p. 1400, Apr. 2021.

[23] J.-W. Zha, Z.-M. Dang, W.-K. Li, Y.-H. Zhu, and G. Chen, "Effect of micro-Si_3N_4-nano-Al_2O_3 co-filled particles on thermal conductivity, dielectric and mechanical properties of silicone rubber composites," *IEEE Trans. Dielectr. Electr. Insul.*, vol. 21, no. 4, pp. 1989–1996, Aug. 2014.

Lívia C. dos Passos Araújo was born in Itajubá, Minas Gerais, Brazil. She received the bachelor's degree in chemistry from the Federal University of Alfenas (UNIFAL), Alfenas, Brazil, in 2015, and the Master of Science degree in materials for engineering from the Federal University of Itajubá (UNIFEI), Itajubá, where she is currently pursuing the Ph.D. degree in materials for engineering.

Her research interests include the applications of silver nanoparticles for polymeric insulators.

Maria E. Leyva was born in Santa Clara, Cuba. She received the bachelor's degree in chemistry from the Universidad de Las Villas-Santa Clara, Santa Clara, Cuba, in 1993, and the M.Sc. and D.Sc. degrees from the Federal University of Rio de Janeiro, Rio de Janeiro, Brazil, in 1999 and 2003, respectively.

She is a Professor of chemistry with the Federal University of Itajubá (UNIFEI), Itajubá, Brazil. Her main research interest concerns in polymer science area, acting on the following subjects: graphene, polyaniline, rubber powder, and nanocomposites.

Estácio T. Wanderley Neto was born in Campina Grande, Brazil, in 1977. He received the bachelor's degree in electrical engineering from the Federal University of Paraíba, João Pessoa, PB, Brazil, in 2001, and the Ph.D. degree in electrical engineering from the Federal University of Campina Grande (UFCG), Campina Grande, Brazil, in 2007.

He was a Professor with UFCG, for two years. He is currently with the Federal University of Itajubá (UNIFEI), Itajubá, Brazil.

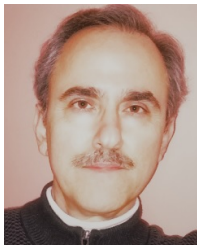

Alvaro A. A. de Queiroz was born in São Paulo, Brazil. He received the Licensure and B.Sc. degrees in sciences (mathematics and chemistry) from the Faculdade de Filosofia Ciências e Letras Farias Brito (FFCLFB), Guarulhos, Brazil, in 1986, the Ph.D. degree in nuclear sciences from the Instituto de Pesquisas Energéticas e Nucleares (IPEN) da Universidade de São Paulo (USP), São Paulo, Brazil, in 1993, and the B.Sc. degree in computer engineering from the Universidade Cruzeiro do Sul (UNICSUL), São Paulo, in 2023.

He was a Full Professor with the Department of Physics and Chemistry, Federal University of Itajubá (UNIFEI), Itajubá, Brazil, where he worked for three decades, retiring in 2018. He is currently a Volunteer Researcher with the Institute for Energy and Nuclear Research (IPEN), São Paulo. He has more than four decades of research and development experience in materials synthesis. His current interest focuses on the development of technologies for DNA digital data storage.